GPS Solut (2007) 11: 61–69
DOI 10.1007/s10291-006-0033-9

ORIGINAL ARTICLE

Anh Quan Le
Christian Tiberius

Single-frequency precise point positioning with optimal filtering

Received: 17 January 2006
Accepted: 2 June 2006
Published online: 11 July 2006

A. Q. Le (✉) · C. Tiberius
Delft Institute of Earth Observation and Space Systems (DEOS),
Delft University of Technology,
Kluyverweg 1, 2629HS Delft,
The Netherlands
E-mail: a.q.le@tudelft.nl

Abstract The accuracy of standalone GPS positioning improved significantly when Selective Availability was turned off in May 2000. With the availability of various public GPS related products including precise satellite orbits and clocks, and ionosphere maps, a *single-frequency* standalone user can experience even a further improvement of the position accuracy. Next, using carrier phase measurements becomes crucial to smoothen the pseudorange noise. In this contribution, the most critical sources of error in *single-frequency* standalone positioning will be reviewed and different approaches to mitigate the errors will be considered. An optimal filter (using also carrier phase measurements) will be deployed. The final approach will then be evaluated in a decently long static test with receivers located in different regions of the world. Kinematic experiments have also been performed in various scenarios including a highly dynamic flight trial. The accuracy, in general, can be confirmed at 0.5 m horizontal and 1 m vertical, with static tests. Ultimate results demonstrate an accuracy close to 2 dm (95%) for the horizontal position components and 5 dm (95%) for the vertical in the flight experiment.

Keywords Precise point positioning · Single-frequency · Filtering

Introduction

Satellite orbits and clocks, together with the atmosphere are currently the main sources of error for standalone GPS positioning after the switch-off of Selective Availability (SA) (Satirapod et al. 2001). With the availability of various GPS related products including GPS orbit and clock products, and Global Ionosphere Maps (GIM) from the International GPS Service (IGS), the standalone positioning accuracy can now be improved to decimeter level with single-frequency and to centimeter level with dual-frequency observations. For *dual-frequency* users, the Precise Point Positioning (PPP) approach was discussed and centimeter-level positioning was demonstrated in static mode (Kouba and Héroux 2001) Several researchers have elaborated on the *single-frequency* approach. Among them, (Øvstedal 2002) discussed different ionospheric models with a 1-week static test validation and (Lachapelle et al. 1996) performed airborne flight tests. Neither of the above-mentioned references could reach sub-meter accuracy at the 95% level of error. More recently (Beran et al. 2005), and (Muellerschoen et al. 2004) demonstrated better accuracy with single-frequency receivers. While the first reference considers mainly short time spans, the second one's approach highly depends on the ionosphere and multipath conditions of the station, which are difficult to be determined.

In this paper, the accuracy of *single-frequency* standalone positioning will be demonstrated by fully exploiting the IGS products together with a more accurate tropospheric model and optimal use of carrier phase measurements. An extensive validation of the accuracy in both static and kinematic modes will be carried out, including flight trials.

Error modeling

Single-frequency point positioning model

The GPS pseudorange observation equation is given as:

$$P_r^s = \rho_r^s + c\delta t_r - c\delta t^s + I_r^s + T_r^s + \varepsilon$$

with P_r^s the observed pseudorange; $\rho_r^s = \|x^s - x_r\|$ the geometric range between receiver and satellite; x^s, δt^s the satellite coordinates and clock error at time of transmission; x_r, δt_r the receiver coordinates and clock error at time of observation; I_r^s, T_r^s the ionospheric and tropospheric delay; ε the unmodeled error (including noise and multipath); and c the speed of light in vacuum.

Collection of all in-view satellites' observations and linearization of the equations will form the mathematical model. The variance-covariance matrix of the observations, with the assumption that pseudorange observables are mutually uncorrelated, is a scaled unit matrix or a diagonal matrix commonly with the (squared) broadcast User Range Accuracies (URAs) as the diagonal elements. However, this latter assumption seems to be inadequate for satellites at low elevation angles. The signal received at a low elevation angle can be more affected by multipath, ionosphere, troposphere errors and receiving antenna gain pattern; and thus the observation is less accurate and should have less weight in the solution. A more appropriate approach is using a so-called "elevation angle dependent weighting function" which is inversely proportional to the sine of the elevation angle. Generally, the standard deviation of a satellite at 5 or 10 degrees is about 10 or 5 times larger than that of a satellite at zenith, respectively (Parkinson and Spilker 1996).

Satellite orbits and clocks

The IGS, since 1994, has been providing several types of precise satellite orbits and clocks, including Ultra Rapid (IGU), Rapid (IGR) and Final (IGS) ephemerides (IGS 2005). They are different in latency and accuracy with the same sampling interval of 15 min. All these products are distributed in SP3 format (Remondi 1993) in which combined satellite positions and clocks are given in tabular form, currently in ITRF2000, an Earth-Centered, Earth-Fixed (ECEF) frame which agrees with the WGS84 at the few centimeter level. An interpolation is needed to get the satellite position at the desired epoch. Schenewerk (2003) shows that an 11-term polynomial interpolator (in the ECEF frame) is suited for this purpose and it is used in this paper.

The fact that the precise satellite positions supplied by IGS are referred to the center of mass, and not to the antenna phase center, makes it more difficult to deal with. In the sense of standalone positioning, a few decimeters of effect can be neglected as in this case. It is assumed that the satellite antenna offset in the body X-coordinate direction can be neglected and there is only the offset in the body Z-coordinate direction which points to the center of the Earth. This assumption leaves a zero X-offset for block IIR and an offset less than 30 cm for block II/IIA, which results in a small range error. The Z-offset can be easily corrected without real knowledge of the satellite body reference frame as the phase center and the mass center are on the same line towards the center of the Earth and the phase center is just 1.023 m closer to the Earth in the block II/IIA case.

Besides the 15-min interval products embedded in SP3 format, satellite clocks are also available as a separate product with a smaller sampling interval, at 5 min. This product is provided in RINEX clock format accompanying the SP3 file and can significantly improve the accuracy of interpolated values, especially where the tabulated values are not regular and gaps occur.

Recently, high-rate satellite clocks also have been made available but only by individual IGS centers, for instance from CODE (CODE 2005). With a 30-s sampling interval, this product can be used to quantify interpolation errors of using 5-min and 15-min products.

Figure 1 shows the interpolation errors due to the Lagrange 11-term polynomial characteristics with the 95th percentile value less than one decimeter. Montenbruck et al. (2005) showed a similar error margin with linear interpolation. In this paper, IGS 5-min clocks with 11-term polynomial interpolation will be used, unless otherwise stated.

A more detailed comparison between different satellite clock products can be found in (Montenbruck et al. 2005).

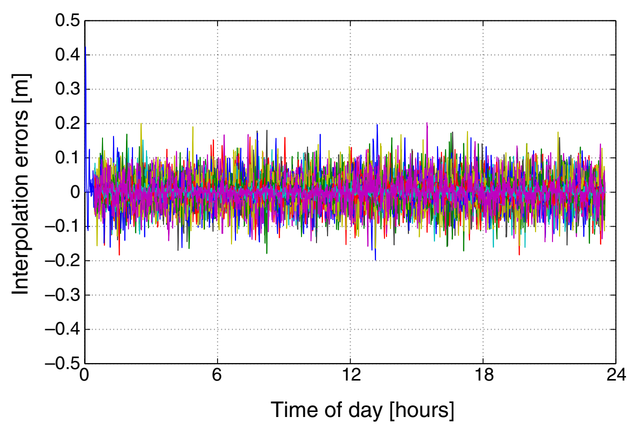

Fig. 1 Interpolation error by going from 5-min (re-sampled) to 30-s clocks (using the CODE 30-s clocks) [m]. Example for January 8, 2003 with all GPS satellites

Ionosphere modeling

The ionosphere is, indeed, the dominant source of error after SA. Although dual-frequency users can easily resolve this problem, ionospheric models still need to be developed for single-frequency users. The range delay can be as large as 100 m at low elevation angles.

The Global Ionosphere Maps (GIMs) have recently become official IGS products. Currently, only 2-dimensional maps are available in which vertical total electron content (TEC) values are provided at geographical grid points (Schaer et al. 1998). Thirteen maps are available given for 24 h with 2-h time spacing. A mapping function is deployed to map the vertical TEC value to the slant TEC value to get the ionosphere correction (Schaer 1999). Due to unavailability of the IGS products at the time of data collection (back to early 2003), the GIMs from CODE are used instead (CODE 2005).

Troposphere modeling

The troposphere delay varies as a function of temperature, pressure, humidity and of course, the actual path along which the signal propagates. There are two main parts of the tropospheric delay, namely the dry and wet delay.

The Saastamoinen model is used in this paper for zenith delays together with the Ifadis mapping functions, see e.g. (Kleijer 2004). The meteorological parameters (surface temperature and pressure) as well as the height above mean sea level are required for the troposphere slant delay computation. Instead of applying default meteorological values of the standard atmosphere, more realistic temperature and pressure values follow from taking the latitudinal and seasonal variations into account; the minimum operational performance standards (MOPS) model is one like this (DO-229A 1998). The temperature and pressure mean values are interpolated (linearly between two neighboring values) from a latitudinal profile and then a model of seasonal variation is applied.

Differential code biases

Different types of codes as well as different frequencies of signals imply different hardware biases, which are generally referred to as differential code biases (DCB). The difference between frequencies (L1 and L2) is called P1-P2 DCB while the difference between code types (on the L1 frequency) is labeled P1-C1 DCB (CODE 2005). For consistency reason (either broadcast or precise), satellite orbits and clocks always refer to the ionosphere-free linear combination of the P1 and P2 code. Hence, single-frequency users must apply the satellite P1-P2 DCBs to get the proper satellite clock information on the frequency of choice.

The P1-P2 DCBs are the differential code biases between the two frequencies and consistent with the P1 and P2 code measurements. However, some receivers do not output the P1 code but the C/A code instead. Therefore, the P1-C1 DCB is needed to adopt the satellite clock information with the C/A code.

The P1-P2 DCBs are included together with the GIMs in IONEX format, but the P1-C1 DCBs are not. They are obtained in a separate file from CODE in this research.

Actually, hardware biases occur at both satellite and receiver. However, the biases at the receiver are absorbed by the receiver clock error in the estimation and do not affect the positioning result.

Carrier-based pseudorange filtering

Since the pseudorange measurement noise is relatively large in comparison to the carrier phase noise, carrier phase measurements can be used to 'average out' the pseudorange noise and provide a more precise result. For this purpose, the phase-smoothed pseudorange algorithm first introduced in (Hatch 1982) can be used. Based on the assumption that the *changes* in carrier phase and pseudorange over a certain interval are equal but carrier phase observations are determined with much higher precision, the current pseudorange can be smoothed[1] by using the carrier phase single difference between epochs on a single-channel basis. However, this algorithm, strictly speaking, only can work with the assumption that the variances of carrier phase observables all equal zero and there is no satellite redundancy; only then it is optimal, see (Teunissen 1991). This is not realistic in GPS positioning where currently much more than four satellites are observed.

Another method, namely the phase-connected pseudorange algorithm was developed in (Bisnath et al. 2002). This algorithm takes the time-differenced carrier phase observations (between epochs) together with the undifferenced pseudorange measurements as basic observations. As long as no cycle slips occur, ambiguity parameters are absent. However, the time-differenced carrier phase observations are highly correlated even if the undifferenced ones are not. This is obviously ignored in the model so that the solution can be computed recursively (Le 2004).

[1]Strictly, *smoothing* implies the computation of estimates for unknown parameters (e.g. position coordinates) pertaining to epoch t_k, using observations from the whole data collection period, i.e. $[t_1, t_l]$ with $1 \le k \le l$; the data period extends beyond epoch t_k. *Filtering* refers to estimates for parameters at epoch t_k, using solely data up to and including epoch t_k, i.e. $[t_1, t_k]$. Filtering allows real-time operation and smoothing does not. In this paper, we continue to refer to 'phase smoothing', as commonly done, but strictly filtering is meant instead.

The optimal solution would be an approach where all the observations (including carrier phase measurements) are put into a unique model of observation equations. This is the model where all the information should be preserved and the unknowns at each epoch can be computed by a recursive least-squares solution. Based on this criterion, the phase-adjusted pseudorange algorithm was developed by (Teunissen 1991). In this model, all original (undifferenced) pseudorange and carrier phase measurements are the basic observations; the unknowns, including ambiguities and positioning parameters, are recursively estimated.

A further comparison of the different algorithms for carrier-based pseudorange smoothing is made in (Le and Teunissen 2006); this reference also presents experiment results.

Cycle slip and outlier detection

Statistical hypothesis testing can be used for cycle slip and outlier detection purposes (Baarda 1968). For single epoch positioning, however the mathematical model is not very strong due to the relatively small redundancy and the low precision of the observations. With sequential epochs, especially after convergence of the recursive least-squares estimation, both observation precision (of the estimated ambiguities) and redundancy are improved making the statistical testing much more powerful.

A local overall model (LOM) test is carried out to detect cycle slips and outliers in the observations (with the level of significance $\alpha = 2.5\%$). The adjective 'local' refers to epoch-by-epoch testing. If the test is rejected, data snooping (w-test) is put into operation. The observation with the maximum (absolute) w-test statistic value is normally the suspected measurement with either a (pseudorange) outlier or a (carrier phase) cycle slip and will be removed (adaptation phase). The remaining data of the epoch will be reprocessed until the LOM test is accepted or the redundancy is zero. After a cycle slip has been found in a particular channel (satellite), the filter is restarted for that channel. A new ambiguity for the satellite will be initialized. This is the DIA-procedure (detection, identification and adaptation) developed by (Teunissen 1990).

Figure 2 shows an example of the beneficial impact statistical testing can have in the case of cycle slips occurrence. The results were from a NovAtel OEM3 receiver, which experienced a loss-of-lock event and slips occurred in *all* phase measurements with not-very-large but different numbers of cycles. The data (1 h span, 1 s interval) were processed twice, once without adaptation and the other with adaptation. The accompanying LOM test statistic values are shown in (Fig. 3)

The loss-of-lock event can be recognized clearly from the Figure, at about 1344 hours (i.e. at 1374 hours in the Figure). Without testing (and adaptation), due to the characteristics of the filtering algorithm, the cycle slip effect lasts for a long time and only gradually phases out. On the contrary, with the testing procedure, the phenomenon is detected and the effect is mitigated in the subsequent epochs. The few remaining positioning error peaks in Fig. 2 at right are due to re-initialization.

Evaluation

With all the development so far, the approach is tested in both static and kinematic environments. A software package developed in *Matlab®*, namely *iSPP* is used for the evaluation. It is capable of doing Single-Frequency Precise Point Positioning in (emulated) real-time with various options, including different filters, different types of products as input. For all the results in this paper, the following products/options are used:

- Final IGS (15-min) orbits and (5-min) clocks
- Final CODE GIMs (including P1-P2 DCB)
- Saastamoinen tropospheric model with Ifadis mapping functions
- P1-C1 DCB from CODE (monthly average)
- Phase-adjusted pseudorange algorithm
- Cut-off elevation angle of 5

Note that throughout this paper (especially in figures) the notation '95th%' stands for the 95th percentile value (taken over the whole set of data) of the (absolute) position errors in local North, East and Up, with respect to the known reference coordinates.

Static experiment

An extensive static test was performed for 7 days with four stations, namely DELF, EIJS, DUBO and HOB2. The first two stations are part of the AGRS.NL network in the Netherlands (Marel van der 1998) while DUBO is in Canada and HOB2 is in Australia. The time interval of the data is 30 s. These data are also used in (Le 2004) with the Phase-connected algorithm. The standard deviations of the (linearized and corrected) code and phase are assumed to be 20 cm and 15 cm, respectively, for satellites at zenith. They increase as a function of elevation angle. The phase's standard deviation is that large due to the applied corrections for various error sources (and the corrections have limited accuracy).

Table 1 summarizes the results; the Phase-connected results (Le 2004) are included for comparison. A significant improvement can be seen by going from the Phase-connected to the Phase-adjusted algorithm, especially in the North component. The algorithm gives 10 to 30% better results in the North direction whereas the East

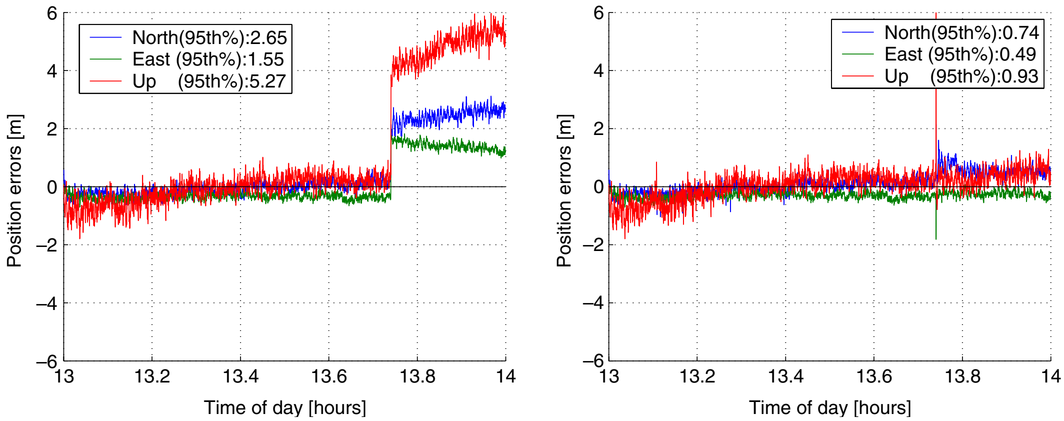

Fig. 2 Position errors with respect to accurately known reference. Time series of North, East and Up components of the NovAtel OEM3 data on Mar 19th, 2005. One hour data, one second interval. *Left* without testing and adaptation. *Right* with testing and adaptation

component's accuracy more or less stays the same. A better accuracy in the vertical direction also can be noticed.

The Phase-adjusted pseudorange algorithm is considered to have converged when the formal accuracy of the estimated ambiguities reaches a certain level. In the static test, it took about 100 epochs for the 10 cm level and 200 epochs for the 5 cm level (standard deviation).

Kinematic experiment: boat trial

The kinematic experiment in (Le 2004) is also reprocessed with the new approach. The test was carried out with a small boat on Schie river (between Delft and Rotterdam, the Netherlands, see Fig.4) Kinematic data from three receivers, namely Ashtech Z-XII3, Leica SR530 and NovAtel OEM3, were collected during nearly 3 h (1 Hz). The cm-accuracy *reference trajectories* were computed in a (dual-frequency carrier phase) differential GPS solution with a reference station nearby (only few kilometers away). Again, the Phase-connected results are included for comparison in Table 2.

Significant improvements of the Phase-adjusted pseudorange algorithm over the Phase-connected algorithm can be seen clearly. For the Ashtech and the Leica receiver, in general, about 20 to 35% better accuracies are obtained in the North component. Whereas, the newly implemented testing procedure detects most of the cycle slips in the NovAtel data and thereby (together with the Phase-adjusted algorithm) improves the (empirical) accuracy by more than 50%.

Kinematic experiment: flight trial

At the end of May and the beginning of June, 2005, two flight tests were carried out with the Cessna Citation aircraft owned by Delft University of Technology together with NLR (Dutch National Aerospace Laboratory) (Fig. 5).

Fig. 3 Local Overall Model test statistic of the NovAtel OEM3 data on Mar 19th, 2005. One hour data, one second interval. The *green line* gives the critical value. *Left* without adaptation. *Right* with adaptation (only first LOM test is shown, regardless any subsequent adaptation)

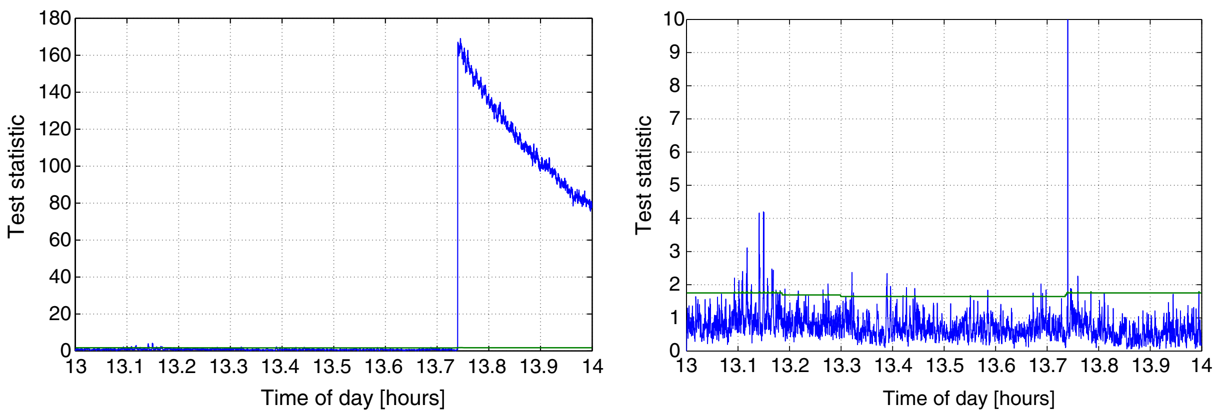

Table 1 The static test results (m). The 95th percentile values of position errors in local North, East and Up coordinates with 1 week of data at 30-s interval for two approaches, four stationary locations around the world

Station	Phase connected	Phase adjusted
DELF		
North	0.56	0.45
East	0.43	0.44
Up	0.93	0.88
EIJS		
North	0.58	0.41
East	0.40	0.42
Up	0.97	0.82
DUBO		
North	0.89	0.78
East	0.55	0.59
Up	1.08	1.01
HOB2		
North	0.66	0.53
East	0.69	0.72
Up	1.61	1.39

Table 2 The single-frequency kinematic results (m). The 95th percentile values of position errors in local North, East and Up coordinates with three different receivers for two approaches, 3 h of data at 1-s interval

Receiver	Phase connected	Phase adjusted
Ashtech Z-XII3		
North	0.68	0.45
East	0.36	0.29
Up	0.80	0.84
Leica SR530		
North	0.49	0.39
East	0.33	0.34
Up	0.72	0.60
NovAtel OEM3		
North	1.44	0.56
East	1.03	0.47
Up	2.83	1.02

There were two flights on two different days, May 31 and June 2, with two receivers on board, a NovAtel EURO4 and a Septentrio PolaRx2@. A summary of the receivers and antennae on the Citation is shown in Table 3.

Dual-frequency data were collected for 2 h on May 31, with both receivers (1 Hz data). For the ground-truth trajectory, a station in Delft equipped with another Septentrio PolaRx2 receiver and a (choke ring) antenna Leica LEIAT504 was used as the reference station. The station (antenna phase center) coordinates are known, and the station is only a few kilometers away from the starting point of the flight trajectory. Figure 6 shows the flight trajectory with respect to the reference station (at the origin of the graph) and the altitude. The aircraft was even below 1,000 meters when flying around the reference station. Then the aircraft climbed to 3,000 meters. The speed of the aircraft was generally between 100 and 150 m/s. The flight was worth 2 h of kinematic data. The *reference trajectories* were computed separately with commercial software, the Trimble Geomatics Office (version #1.62) with (carrier phase) differential positioning. Both L1 and L2 carrier phase data were used to form the ionosphere-free linear combination. Troposphere modeling was crucial in this case where the rover and the reference station were distant and largely different in height. The Niell tropospheric model was chosen with the zenith wet delay estimated. Ambiguities were reported to be resolved successfully.

There were some technical problems in determining the 'ground-truth' for the Septentrio receiver on board

Fig. 4 The boat carrying the three receivers was repeatedly sailing a trajectory of a few kilometers length

Fig. 5 The Cessna Citation II laboratory aircraft of the faculty

Table 3 Receivers and antennae on board the Cessna Citation aircraft (both dual-frequency)

Receiver	Antenna
Septentrio PolaRx2@	Sensor Systems S67-1575-96
NovAtel EURO4 RT2	AIL Dorne-Margolin C146-2-6

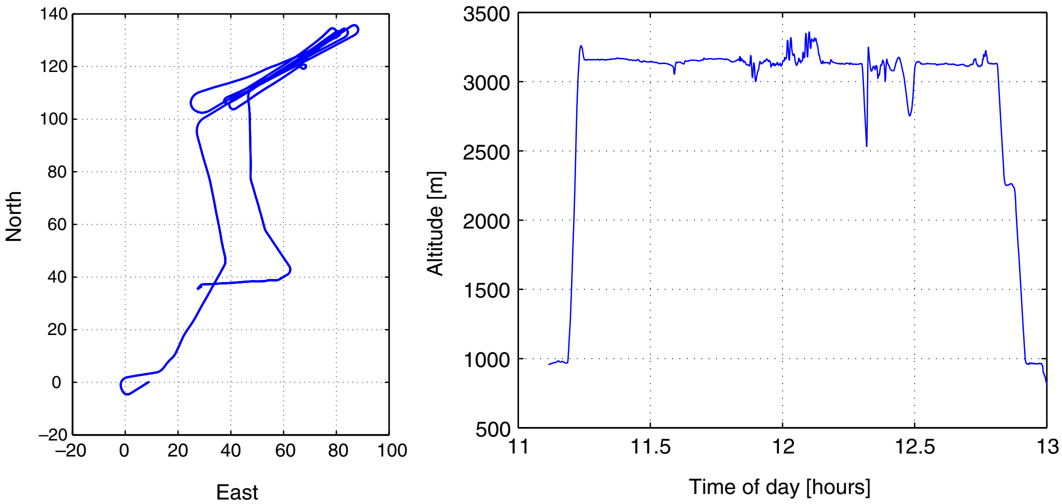

Fig. 6 Trajectory (km) and altitude (m) of the flight on May 31. The reference station is at the origin (in the *left* graph)

the aircraft due to an incompatibility between the Septentrio data (in RINEX) and the Trimble Geomatics Office software. The Septentrio receiver lets its clock drift within 1 ms symmetrically around zero, which means that the clock will be reset to $\pm$ 0.5 ms when it reaches $\mp$0.5 ms (discrete clock jumps and the handling of these clock jumps in the data file does not fully comply with the RINEX standard). Whereas, the NovAtel receiver continuously steers its clock to zero [see e.g. (Le and Tiberius 2003)]. The incompatibility problem occurs when Trimble Geomatics Office seems to work only with one-sided clock offsets, or more precisely, only with negative clock offsets. Thus, only the data with negative clock offsets from the Septentrio receiver can be processed with Trimble Geomatics Office, other parts are marked as gaps. At the beginning, when the baseline was very short, centimeter level is expected for the accuracy of the reference trajectory. This has been verified by an independent check using in-house software. Further away, at larger distance, the accuracy is anticipated to be at decimeter level because of remaining differential atmospheric delays. At the reference station, clock jumps also occurred in the PolaRx2, but it was configured differently (with 5 ms threshold). As it was marked as static in the solution, the clock jumps were detected and removed by the Trimble Geomatics Office without any extra effect.

Now the reference trajectories have been established, the performance of *single-frequency* standalone positioning will be assessed. Note that only the phase-adjusted method is used. Figure 7 shows the result of the NovAtel receiver while the performance of the Septentrio receiver is shown in (Fig. 8). Both receivers give similar accuracies, about 2 dm horizontally and 5 dm vertically (95th%).

From the second flight test on Jun 2, due to technical problems (data logging), only the NovAtel data can be

Fig. 7 Position coordinate errors. Flight results (May 31) from NovAtel EURO4 (2 h with 1 Hz data). *Left* Time series of North, East and Up component (m). *Right* Horizontal scatter (m)

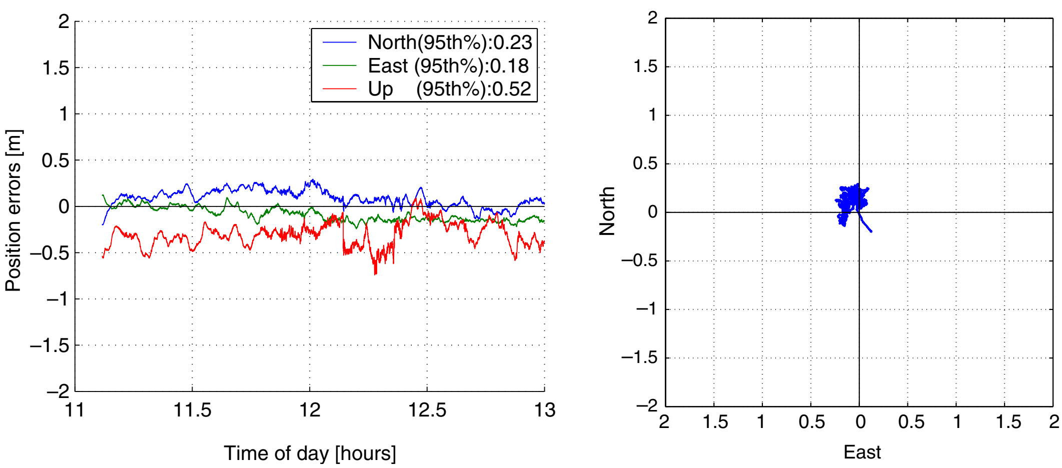

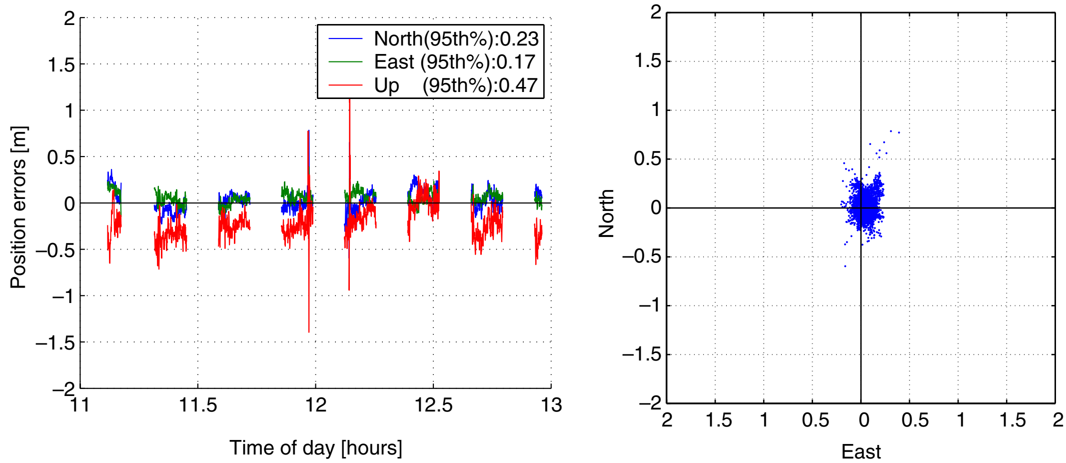

Fig. 8 Flight results (May 31) from Septentrio PolaRx2@ (2 h with 1 Hz data). *Left* Time series of North, East and Up component (m). *Right* Horizontal scatter (m). The gaps are because of missing reference trajectory

used. The reference trajectory was derived in a similar way as in the first flight test.

The results are given in Fig. 9 for a 1-h time span. Due to multiple changes in the satellites used for computing the positions (this flight involved a lot of extreme maneuvers), the accuracy of the height component is not as good as the first flight but still within 1 m (95th percentile).

These results show that the positioning approach works well even with highly kinematic platforms and in a demanding environment. It also can be noted that the convergence in the kinematic tests is similar to that in the static tests, about 100–200 epochs (or 2–3 min in this case).

Fig. 9 Flight results (June 2) from NovAtel EURO4 (1 h with 1 Hz data). *Left* Time series of North, East and Up component (m). *Right* Horizontal scatter (m)

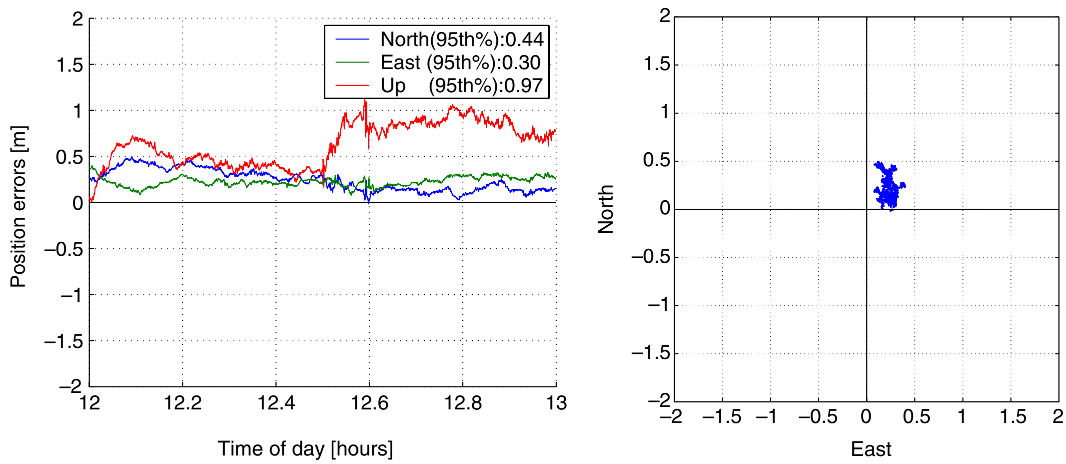

Conclusions

The Phase-adjusted pseudorange algorithm, statistically optimal, is a fully kinematic filter. It has been demonstrated to work robustly in various circumstances, from static to highly kinematic, over short time spans and long time spans. From the results, quick convergence of the filter can be recognized. With the fully implemented Phase-adjusted pseudorange algorithm including statistical testing, the accuracy of the improved single-point positioning, in general, can be confirmed at 0.5 m horizontally and 1 m vertically (at the 95th percentile level). It proves to have a better accuracy than that of the Phase-connected approach, by about 10 to 30%. In favorable conditions, the accuracy gets close to 2 dm horizontally and 5 dm vertically (95th%), and does not depend on the receiver's dynamics.

At this level of accuracy, other sources of errors should be accounted for. They are solid earth tides, ocean loading, phase wind-up and others. The full correction of satellite antenna phase center also should be applied. All those corrections/modeling might bring the accuracy close to sub-decimeter level since the errors are at a few decimeters level in total.

Acknowledgments The flight data (as well as the photograph of the aircraft) were kindly provided by José Lorga of the Control and Simulation division, Faculty of Aerospace Engineering, Delft University of Technology. Also the effort of the aircraft crew is appreciated in performing the special maneuvers.

References

Baarda W (1968) A testing procedure for use in geodetic networks. NCG-publications on geodesy, Vol. 2, No. 5, Delft

Bisnath SB, Beran T, Langley RB (2002) Precise platform positioning with a single GPS receiver. GPS World, April 2002, pp 42–49

CODE (2005). Center for Orbit Determination in Europe. Astronomy Institute, University of Berne. http://www.aiub.unibe.ch/igs.html

DO-229A (1998) Minimum operational performance standards for global positioning system/wide area augmentation system airborne equipment. Document No. RTCA/DO-229A. Prepared by SC-159, 1998

Hatch R (1982) The synergism of GPS code and carrier measurements. In: Proceedings of the 3rd international geodetic symposium on satellite doppler positioning, Vol. 2. Las Cruces–New Mexico, 1982, pp 1213–1231

IGS (2005) International GPS Service. Website http://www.igscb.jpl.nasa.gov/

Kleijer F (2004) Troposphere delay modeling and filtering for precise GPS leveling. Ph.D thesis. Mathematical Geodesy and Positioning, Delft University of Technology

Kouba J, Héroux H (2001) Precise point positioning using IGS orbit and clock products. GPS Solut 5(2):12–28

Lachapelle G, Cannon ME, Qiu W, Varner C (1996) Precise aircraft single-point positioning using GPS post-mission orbits and satellite clock corrections. J Geodesy 70:562–571

Le AQ, Tiberius CCJM (2003).GPS Standard positioning service: how good is it?. Eur J Navig 1(2):21–27

Le AQ (2004) Achieving decimetre accuracy with single frequency standalone gps positioning. In: Proceedings of the ION GNSS 17th International Technical Meeting of the Satellite Division, 21–24 Sept. 2004, Long Beach, pp 1881–1892

Le AQ, Teunissen PJG (2006) Recursive least-squares filtering of pseudorange measurements. In: European navigation conference 2006, 7–10 May 2006, Manchester, (accepted for publication)

Marel van der H (1998) Monitoring of the Dutch active GPS reference system. In: Proceedings of IGS network systems workshop, Annapolis, 2–5 November, 1998, pp 171–172

Montenbruck O, Gill E, Kroes R (2005) Rapid orbit determination of LEO satellites using IGS clock and ephemeris products. GPS Solut 9(3):226–235

Muellerschoen RJ, Iijima B, Meyer R, Bar-Sever Y (2004) Real-time point-positioning performance evaluation of single-frequency receivers using NASA's global differential GPS system. In: Proceedings of the ION GNSS 17th International Technical Meeting of the Satellite Division, 21–24 Sept. 2004, Long Beach, pp 1872–1880

Øvstedal O (2002) Absolute positioning with single frequency GPS receivers. GPS Solut 5(4):33–44

Parkinson BW, Spilker JJ (eds) (1996) Global positioning system: theory and applications vol. 1. Progress in astronautics and aerodynamics. Vol. 163. AIAA, Washington

Remondi BW (1993) NGS second generation ASCII and binary orbit formats and associated interpolation studies. In: IAG Symposia (Symp. 109, Vienna, Austria, August 11–14, 1989) by IUGG, and IAG

Satirapod C, Rizos C, Wang J (2001) GPS single point positioning with SA off: how accurate can we get? Surv Rev 36(282):255–262

Schaer S, Gurtner W, Feltens J (1998) IONEX: the ionosphere map exchange format version 1. Proceedings of the IGS AC Workshop, Darmstadt, February 9–11, 1998

Schaer S (1999) Mapping and predicting the earth's ionosphere using the global positioning system. Ph.D thesis. AIUB, University of Berne

Schenewerk M (2003) A brief review of basic GPS orbit interpolation strategies. GPS Solut 6(4):265–267

Teunissen PJG (1990) Quality control in integrated navigation systems. IEEE Aerosp Electron Syst Mag 5(7):35–41

Teunissen PJG (1991) The GPS phase-adjusted pseudorange. In: Proceedings of the 2nd international workshop on high precision navigation Stuttgart/Freudenstadt, Germany, 1991, pp 115–125